Platform Design and Mathematical Modeling of an Ultralight Quadrotor Micro Aerial Vehicle

Kun Li, Swee King Phang, Ben M. Chen, Tong Heng Lee

Abstract— **In this paper, a micro quadrotor aircraft with approximately 40 g gross weight and 8 min flight endurance is developed. System development of this micro aerial vehicle is discussed in terms of the design of the mechanical structure and electrical systems. Mechanical structure is designed based on the proposed weight budget, propulsion system efficiency as well as results of structural analysis. Mechanical parts are designed and analyzed with 3D simulation software then 3D printed. Development of the electrical systems includes integration of processor, inertia measurement unit, and communications with commercial off-the-shelf electronics. Finally, a mathematical model of the quadrotor is derived based on the quadrotor X-configuration working principle. Parameters involved are further identified with experimental setups or simulations. The controller is first simulated with software simulator and then tuned with real flight tests.**

I. INTRODUCTION

The interest in research of micro aerial vehicle (MAV) has been aroused, as more requirements are casted on unmanned aerial vehicle (UAV) for military tasks of surveillance, reconnaissance and detection in obstacle-rich areas, clandestine military bases, radiant areas and other dangerous regions. These requirements include the needs for intelligence, simultaneous location and mapping, path planning, and obstacle avoidance, as well as long endurance to cover long range flight and communication with ground control station. In the recent few decades, with the improvement of large-scale integrated circuits, the size of the aircraft also triggered much study in the area of MAV, or even nano aerial vehicle (NAV). In 1997, the Defense Advanced Research Projects Agency (DARPA) gave a definition of MAV, which requires maximum dimension of the aircraft in any direction to be no greater than 15 cm, the gross weight should not exceed 100 g, with up to 20 g devoted to payload, and that the aircraft should be able to reach an altitude of 100 m.

Design approaches of MAV include fixed-wing, rotary-wing, flapping-wing and other unconventional platforms. Black Widow, an 80 g fixed-wing MAV developed by AeroVironment, has a 6-inch wingspan and is claimed to be fully autonomous [1]. However, a fixed-wing platform is unable to hover, limiting the aircraft maneuverability in cluttered environments such as narrow corridors, rooms with obstacles. Flapping-wing aircraft is a vertical take-off and landing (VTOL) mechanism, mimicking the behavior of an insect or a bird. A 3 cm size flapping-wing MAV was developed by Harvard University in 2007, to biologically mimic the Dipteran insects [2]. However, a flapping mechanism requires sophisticated mechanical manufacturing and aerodynamic analysis of the wing structure. Ducted-fan platform is also a possible approach for miniature aerial vehicle. In the literature [3], development and modeling of a 150 g platform is described. Nevertheless, it requires extra fins to control its attitude, resulting in difficulty in weight reduction. Therefore, from the perspective of the platform approach, quadrotor platform is developed as the MAV platform in our project due to its maneuverability and mechanical feasibility.

In the literature [4], Stanford University has developed a micro quadrotor 'Mesicopter', with an impressive weight of 3 g. It is, however, unable to take off due to its rotor efficiency problem. Recently, Mellinger and his collaborators from GRASP lab have been working on the formation flight of small scale quadrotor UAVs and have achieved impressive results [5]. It has an high attitude control update rate of 1 kHz, and its position can be controlled with the aid of VICON Motion Capture System.

In this paper, a guideline to design a quadrotor MAV which satisfies DARPA's requirements for MAV is proposed. Large effort was made to investigate the feasibility of overall structure and to evaluate the platform from the weight, size and power consumption with both experiments and simulation before manufacturing.

Main contents of this paper are divided into four sections. Section II shows the hardware development of the overall platform, which includes mechanical structure and electrical system. Section III describes a nonlinear model of the quadrotor concerning kinematics, rigid-body dynamics, and motor model. In section IV, each of the parameter involved in the nonlinear model is identified by experimental or simulation methods. In section V, simulation and real flight test results are shown. Conclusion and future research focus are given in the last section.

II. PLATFORM DESIGN

A. Design Layout and Weight Budget

The mechanical structure layout of this quadrotor helicopter is shown in Fig. 1. Sizing for the aircraft is a tradeoff between the requirements and quadrotor functionality, shown in Fig. 1. Distance of two diagonal rotors is 142.54 mm, with a total height of 38.50 mm. The platform is elevated by the lift forces generated by four rotors with two clockwise spinning propellers (black) and two anti-clockwise spinning

K. Li, B. M. Chen and T. H. Lee are with the Department of Electrical & Computer Engineering, National University of Singapore (NUS), Singapore. E-mail: {kunli89,bmchen,eleleeth}@nus.edu.sg

S. K. Phang is with the NUS Graduate School for Integrative Sciences & Engineering, National University of Singapore (NUS), Singapore. E-mail: king@nus.edu.sg

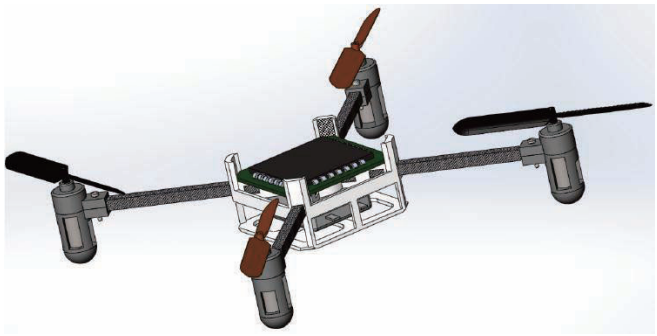

(a)

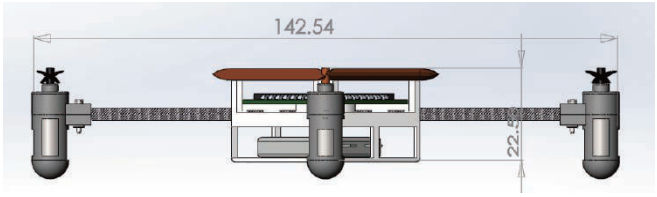

(b)

Fig. 1. Mechanical structure layout and size

propellers (orange). The printed circuit board (PCB) including the processor, inertial measurement unit (IMU) and communications is located in the center of quadrotor's body, sitting on an anti-vibration sponge. A lithium polymer (Li-Po) battery is attached below the PCB as the main power source for the system. Details of weight breakdown are reflected in Table. I.

TABLE I

WEIGHT BUDGET FOR QUAD-ROTOR MAV

Components	Amount	Weight Budget (g)	Current Weight (g)
Battery	1	12	9.90
Motor	4	3	3.34
Propeller	4	0.5	0.25
Motor Holder	4	0.5	0.55
Carbon Fiber Tube	4	0.5	0.38
Frame	1	2	2.60
PCB (IMU & CPU)	1	7	6.89
Communications	1	2	0.23
Camera	1	2	0.82
Video TX	1	3	2.23
Camera PCB	1	1.5	1.1
Contingency	5%	1.5	
Total		49	41.85

B. Motor and Propeller Combo

To provide 3D movements for the aircraft, the lift exerted from the rotors should be more than its own weight at full throttle, as extra thrust is needed during elevation or forward flight. The requirements is higher during aggressive flight. The possible candidates of commercial off-the-shelf COTS motors and propellers are listed in Table. II, where d is the diameter of propeller and C is the chord length. Performances of motor and propeller combo are listed in Table. III. With the consideration of tradeoff between overall component weight and lift created, the option of motor 'ML-3' and 'PL-3' is selected, shown in Fig. 2.

(a) (b)

Fig. 2. Motor and propeller combo

TABLE II

COTS MOTORS AND PROPELLER

Motor	Type	m (g)	**Prop**	d (mm)	C (mm)	m (g)
ML-1	2-cell brushless	3.23	PL-1	81	12	1.01
ML-2	1-cell brushless	2.41	PL-2	65	11	0.52
ML-3	1-cell brushed	3.34	PL-3	56	8.2	0.25

TABLE III

MOTOR AND PROPELLER COMBO

Power	Options	Thrust (g)	ESC
2 Cell	ML-1 & PL-1	26	2-cell brushless
	ML-1 & PL-2	14.5	2-cell brushless
1 Cell	ML-2 & PL-1	19	2-cell brushless
	ML-2 & PL-2	12	2-cell brushless
	ML-3 & PL-2	6.58	1-cell brushed
	ML-3 & PL-3	16.4	1-cell brushed

C. Structural Analysis

For a small scale flying object, especially rotary-wing aircraft, its resonant frequencies will heavily affect the platform stability and performance. Several frame structures have been considered and compared based on their resonant frequencies analysis. The main material for the frame is carbon-fiber (CF) reinforced polymer, with high tensile strength-to-weight ratio, which is appropriate for micro aircraft frame. Mechanical properties for the uni-directional carbon and epoxy of type T300/976 are listed in Table. IV. This material is strong in forward direction and weak in lateral, ideal to be used as cantilever beams, which act as the micro quadrotor arms.

A simplified model for cantilever beam first natural frequency model calculation is given by,

$$f_1 = \frac{1}{2\pi}\sqrt{\frac{3EI}{mL^3}}, \tag{1}$$

where E is the Young's Modulus, ρ is the density, m is the mass of load attached to the end of beam, and I is the moment of the cross-section. Several cross-section shapes

TABLE IV

MECHANICAL PROPERTIES FOR T300/976 CARBON/EPOXY

Description	Symbol	T300/976
Young's Modulus along Grain	E_1(GPa)	135.2
Poisson Ratio along Grain	v_{12}	0.32
Shear Modulus along Grain	G_{12}(GPa)	6.28
Density	ρ(kgm^{-3})	1480

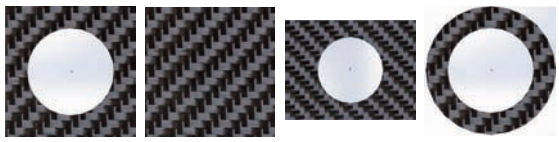

(a) (b) (c) (d)

Fig. 3. Cross-section shapes of CF beam

of the cantilever beam are shown in Fig. 3. Frequency analysis simulations were conducted to find one with high resonant frequency to prevent any mechanical resonance with the motor's working frequency. Four 60 mm length CF beam with shapes including square tube (cross-section 3×3 mm with 2 mm round hollow), square bar (cross-section 3×3 mm), rectangular tube (cross-section 4×3 mm with 2 mm round hollow) and round tube (3 mm/2 mm) were tested. The results reflect that square tube obtains the highest fundamental resonant frequency, listed in Table. V.

TABLE V

FREQUENCY ANALYSIS OF 4 CF CROSS-SECTION SHAPE

Shape	T300/976 (Hz)	Weight (g)
Shape A	1566.2	0.499
Shape B	1345	0.663
Shape C	1537.9	0.753
Shape D	1193.8	0.293

For the overall structure, previous prototypes adopted a simple framework which made two CF tubes perpendicular to each other at the center. It was found that this structure was subject to vibrations at the working range of rotor speed. Therefore, a structure of four single CF arms fastened by a fixed mount at the center is proposed. Frequency analysis of these assembly parts are shown in Fig. 4, where the fundamental resonant frequency of the current structure is 1199.6 Hz, compared with the previous frame, 785.48 Hz. The legend in Fig. 4 shows the vibration amplitude of different parts of the frame under the resonant frequency. The current natural frequency, far away from the rotor's highest frequency of 300 Hz, is high enough to prevent the platform from resonance.

The structure in Fig. 1 is an assembly part with four CF tube beams and a mount part made of acrylonitrile butadiene styrene (ABS) plastic by 3D printing. This is a stable and more integrated structure, of which an optimal length for each CF beam can be achieved. An experiment was

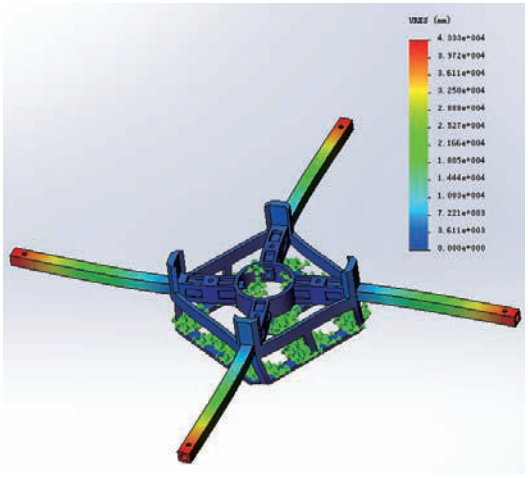

Fig. 4. Overall structure analysis

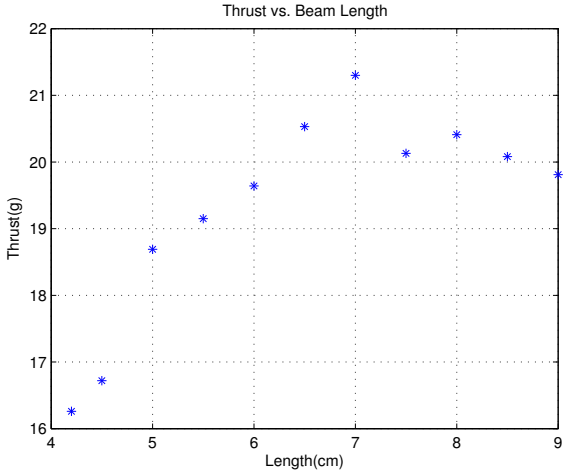

Fig. 5. Beam length vs. lift

conducted to find the relationship between CF beam length and total thrust exerted from four motor mounted on each end of a CF tube cross. The result, shown in Fig. 5, indicates that when the distance from center of gravity (CG) to center of motor decreases below 7 cm, interference between air flow of adjacent rotors emerges, resulting in reduction of the total thrust. Thus, a 7 cm distance is desirable.

D. Avionic System Design

The Attitude and Heading Reference System (AHRS) is the most significant sensor onboard the helicopter, generally consisting of a 3-axis gyroscope, a 3-axis accelerometer and a magnetometer. This AHRS system provides real-time attitude and heading information, used as feedback for the aircraft to achieve stability. For this minimalist quadrotor aircraft design, a commercial product with small scale, light weight and accurate sensing is more preferred rather than developing the sensing system by ourselves. Also, as the size of aircraft decreases, the dynamic property of the vehicle becomes faster and high updating-rate AHRS system is desired. To strike a balance between the AHRS performance and weight and size requirements, ArduIMU series and

(a) (b) (c)

Fig. 6. AHRS commercial products

VectorNAV VN-100 become possible candidates.

ArduIMU V2 (Fig. 6(a)) is a low-cost IMU with a 3-axis accelerometer ADXL335, an x- and y-axis gyroscope LPR530AL, a z-axis gyroscope LY530ALH without internal magnetometer. These analog inputs are processed by an Atmega328 with Direct Cosine Matrix (DCM) algorithm to obtain attitude. ArduIMU V3 (Fig. 6(b)) replaces the gyroscope and accelerometer in V2 with MPU6000 and adds an internal magnetometer HMC5883L, while the processor remains the same. VectorNav VN-100 (Fig. 6(c)) is a miniature, light weight, low power high-performance AHRS in a surface mount package and incorporates the latest solid-state MEMS technology. The basic features of these IMUs are listed in Table. VI. From the specifications comparison and comprehensive design requirements, the VN-100 from VectorNav outweighs the other two versions from ArduIMU.

TABLE VI

IMU SPECIFICATIONS COMPARISON

Description	VN-100	ArduIMU V2	ArduIMU V3
Frequency	200 Hz	70 Hz	70 Hz
Sensors	Gyro, accelerometer, magnetometer	Gyro, accelerometer	Gyro, accelerometer, magnetometer
Processor	32-bit	8-bit	8-bit
Dimension (mm)	$22 \times 24 \times 3$	$39 \times 28 \times 3$	$38 \times 25 \times 3$
Package	Surface mount	PCB	PCB
Weight (g)	3	6.03	3.90
Communications	2 UART, SPI	UART	UART

A PCB incorporating the VN-100, a 8-bit processor ATmega328p, four 1-cell brushed ESC is designed to perform the sensor reading, control and output pulse-width modulation (PWM) values to four rotors. Figure 7(a) and 7(b) show the front and reverse side of the PCB. DT receiver working with Spectrum DSM2 transmitter is selected as the communication module. Its specifications are listed in Table. VII.

Based on the electrical components choices, an overall power consumption analysis is conducted to calculate the power needed to maintain 8 minutes flight. Table. VIII records the current and power consumption of motors and electronics at their rated voltage. The total power consumption at the hovering status is approximately 7 watt under rate voltage of 3.7 V. Based on the calculated energy needs to be provided, a single cell 360 mAh Li-Po is able to maintain 8 min flight. Here a 3.7 V 360 mAh Li-Po battery from

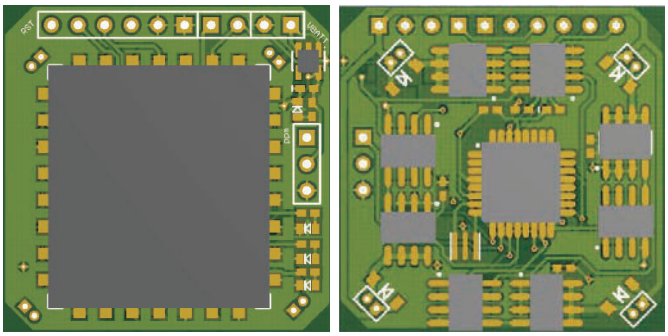

(a) (b)

Fig. 7. Printed circuit board view

TABLE VII

DT RECEIVER RX31D

Description	Specification
Outputs	4, Servos, 1024 step
Optional output	7 ch sum-PPM and serial output on 1 pin
Size	$9.8 \times 10.2 \times 2.2$ mm
Weight	0.24 g
Voltage Supply	3-6 V

Hobbyking is selected to maintain 8 minutes flight.

TABLE VIII

POWER CONSUMPTION ANALYSIS

Components	Rated Voltage (V)	Current (A)	Power (W)
4 Motor & ESC	3.8	1.64	6.232
CPU	3.3	0.022	0.074
Communications	3.3	0.075	0.249
AHRS	3.3	0.088	0.292
5% Buffer	3.3		0.164

The completely assembled platform is shown in Fig. 16 and Fig. 17.

III. MATHEMATICAL MODELING

Two coordinate frames, north-east-down (NED) frame $\begin{bmatrix} x_n & y_n & z_n \end{bmatrix}$ and the body frame $\begin{bmatrix} x_b & y_b & z_b \end{bmatrix}$, will be considered [6]. The NED frame is stationary with respect to a static observer on the ground. The body frame is the coordinate frame with the origin located at the CG with its orientation moving together with the aircraft fuselage.

Mechanical layout of the quadrotor MAV is the X-configuration, the basic working principle of which is described in Fig. 9. T_1, T_2, T_3 and T_4 are the lift force created by rotor 1, 2, 3 and 4 (front-right, rear-right, rear-left, front-left rotor respectively). Rotor 1 and 3 rotate clockwise and rotor 2 and 4 rotate counter-clockwise, resulting in zero net-moment when hovering. Combinations of different angular speed of each rotor result in pitch, roll and yaw motions.

The overall structure view of this quadrotor platform can be described as Fig. 8, where δ_{ail}, δ_{ele}, δ_{thr}, and δ_{rud} represent the input signals from aileron, elevator, throttle and rudder channels, respectively. Different channel inputs from the

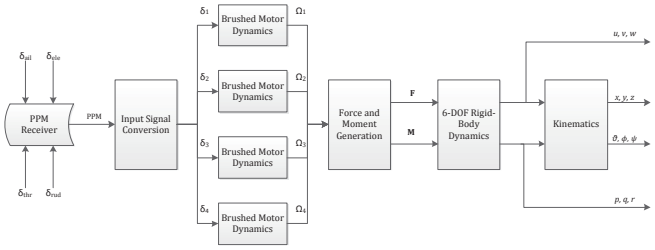

Fig. 8. Overall structure of the quadrotor

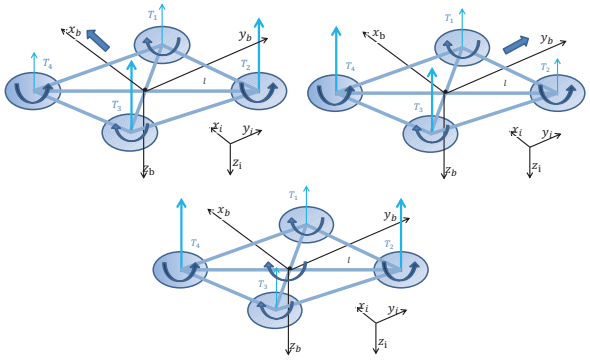

Fig. 9. X-configuration working principle

transmitter are coded as PPM signal and sent to onboard system via the receiver. δ_1, δ_2, δ_3 and δ_4 are the PWM values input to each motor and Ω_1, Ω_2, Ω_3 and Ω_4 are motors' individual rotational speeds. $\mathbf{V_b} = \begin{bmatrix} u & v & w \end{bmatrix}^T$ are linear velocities in body frame x_b, y_b and z_b directions respectively. Angular rate of $\omega = \begin{bmatrix} p & q & r \end{bmatrix}^T$ can be obtained by 6 degree-of-freedom (DOF) rigid body dynamics, and position in NED frame $\mathbf{P_n} = \begin{bmatrix} x & y & z \end{bmatrix}^T$ and Euler angles $\Theta = \begin{bmatrix} \phi & \theta & \psi \end{bmatrix}^T$ can be calculated through kinematics.

A. Kinematics

With respect to the stationary NED frame, the aircraft has translational and rotational motions such that it can be represented in a transformation matrix between the two frames mathematically [7]. Equation (2) and (3) represent the navigation equations applicable to transformation between the two frames:

$$\dot{\mathbf{P}}_\mathbf{n} = \mathbf{R}_{\mathbf{n/b}}\mathbf{V_b}, \tag{2}$$

$$\dot{\Theta} = \mathbf{S^{-1}}\omega, \tag{3}$$

where $\mathbf{R_{n/b}}$ represents the transformation matrix and $\mathbf{S^{-1}}$ is given by:

$$\mathbf{R_{n/b}} = \begin{bmatrix} c_\theta c_\psi & s_\phi s_\theta c_\psi - c_\phi s_\psi & c_\phi s_\theta c_\psi + s_\phi s_\psi \\ c_\theta s_\psi & s_\phi s_\theta s_\psi + c_\phi c_\psi & c_\phi s_\theta s_\psi - s_\phi c_\psi \\ -s_\theta & s_\phi c_\theta & c_\phi c_\theta \end{bmatrix}, \tag{4}$$

$$\mathbf{S^{-1}} = \begin{bmatrix} 1 & s_\phi t_\theta & c_\phi t_\theta \\ 0 & c_\phi & -s_\phi \\ 0 & s_\phi / c_\theta & c_\phi / c_\theta \end{bmatrix}, \tag{5}$$

where $s_* = \sin(*)$, $c_* = \cos(*)$, $t_* = \tan(*)$.

B. 6 DOF Rigid Body Dynamics

Based on Newton-Euler formalism describing the translational and rotational dynamics of a rigid body, the dynamic equations can be written into input-output form [8]:

$$m\dot{\mathbf{V}}_\mathbf{b} + \omega \times (m\mathbf{V_b}) = \mathbf{F}, \tag{6}$$

$$\mathbf{J}\dot{\omega} + \omega \times (\mathbf{J}\omega) = \mathbf{M}, \tag{7}$$

where $\mathbf{F}$ and $\mathbf{M}$ are the force and moment vectors, $\mathbf{J}$ is the inertia moment of the aircraft:

$$\mathbf{J} = \begin{bmatrix} J_{XX} & J_{XY} & J_{XZ} \\ J_{XY} & J_{YY} & J_{YZ} \\ J_{XZ} & J_{YZ} & J_{ZZ} \end{bmatrix}. \tag{8}$$

C. Forces and Moments

Based on the working principle of the quadrotor [9], the forces and torques are mainly generated by the four rotors [10]. The following equation represents the components part of the overall force and moment vector:

$$\Lambda = \begin{bmatrix} \mathbf{F} \\ \mathbf{M} \end{bmatrix} = \Lambda_g + \Lambda_r + \Lambda_{rt}, \tag{9}$$

where Λ_g, Λ_r, and Λ_{rt} are forces and moments generated by gravity, rotors and propellers as well as reactional torque.

1) Gravity Factor: As the platform is x-axis and y-axis symmetric, the CG is located on the z-axis, thereby the gravitational force only contributes to the force vector. Considering the coordinate frames, the gravity only exists on the z-axis in NED frame and need to be transformed to body frame by the transformation matrix:

$$\mathbf{F_g} = \mathbf{R_{n/b}}^{-1} \begin{bmatrix} 0 \\ 0 \\ mg \end{bmatrix} = \begin{bmatrix} -mgs_\theta \\ mgc_\theta s_\phi \\ mgc_\theta c_\phi \end{bmatrix}, \tag{10}$$

giving that,

$$\Lambda_g = \begin{bmatrix} \mathbf{F_g} \\ 0 \end{bmatrix} = \begin{bmatrix} -mgs_\theta \\ mgc_\theta s_\phi \\ mgc_\theta c_\phi \\ 0 \\ 0 \\ 0 \end{bmatrix}. \tag{11}$$

2) Motors and Propellers: The motors and propellers are the main source of forces and moments generation. Propellers with reverse configurations are mounted on each two beams of the cross to counter the rotational torques produced by each other. As in [11], let T_i and Q_i be the thrust and torque created by n-th motor and propeller pairs, $(i = 1,2,3,4)$, they can be expressed as below:

$$T_i = C_T \rho A (\Omega_i R)^2, \tag{12}$$

$$Q_i = C_Q \rho A (\Omega_i R)^2 R, \tag{13}$$

where C_T and C_Q are the propeller aerodynamic coefficient, ρ is the air density, A is the area of the propeller swept by the rotating rotor and R is the radius of the rotor A. Assuming that the distortion of the propellers during high frequency

rotation can be ignored, Eq. (12) and (13) can be simplified as:

$$T_i = k_T \Omega_i^2, \quad (14)$$
$$Q_i = k_Q \Omega_i^2, \quad (15)$$

where these two coefficients k_T and k_Q can be obtained by a series of experiments. Thereby, the sum of these four thrusts will result in a total thrust in -z-axis in the body frame, as below:

$$\mathbf{F_r} = \begin{bmatrix} 0 \\ 0 \\ -(T_1+T_2+T_3+T_4) \end{bmatrix}. \quad (16)$$

The moments are generated when the four generated forces have different magnitudes and result in pitch, roll and yaw movements. The moment component product contributed by rotors is calculated as:

$$\mathbf{M_r} = \begin{bmatrix} \frac{\sqrt{2}}{2} l(T_2+T_3-T_1-T_4) \\ \frac{\sqrt{2}}{2} l(T_1+T_2-T_3-T_4) \\ Q_1-Q_2+Q_3-Q_4 \end{bmatrix}, \quad (17)$$
$$= \begin{bmatrix} \frac{\sqrt{2}}{2} k_T l(\Omega_2^2+\Omega_3^2-\Omega_1^2-\Omega_4^2) \\ \frac{\sqrt{2}}{2} k_T l(\Omega_1^2+\Omega_2^2-\Omega_3^2-\Omega_4^2) \\ k_Q(\Omega_1^2-\Omega_2^2+\Omega_3^2-\Omega_4^2) \end{bmatrix}, \quad (18)$$

where l is distance from center of the motor to the platform CG.

3) Reaction Torque: The first-order derivative of rotational movement can cause the inertia counter torque, and this torque only affect the movement in yaw direction, which is

$$\Lambda_{rt} = \begin{bmatrix} 0 \\ \mathbf{M_{rt}} \end{bmatrix} = \begin{bmatrix} 0 \\ 0 \\ 0 \\ 0 \\ 0 \\ -J_r(\dot{\Omega}_1-\dot{\Omega}_2+\dot{\Omega}_3-\dot{\Omega}_4) \end{bmatrix}, \quad (19)$$

where J_r is the moment inertia of the rotor. The overall forces and moments are the summation of the above-mentioned factors, just as described in Eq. 9.

D. Brushed Motor Dynamics

The brushed motor is controlled by a single cell brushed electronic speed controller. The transient property of this brushed motor can be approximated as a first order process, as shown below:

$$\dot{\Omega} = \frac{1}{\tau_m}(k_m u - \Omega), \quad (20)$$

where u is the input, τ_m and k_m are the time constant and process gain of the first-order model.

E. Input Signal Decoding

Input PPM signals contain information of aileron, elevator, throttle and rudder channel, which can be decoded as:

$$\begin{bmatrix} \delta_1 \\ \delta_2 \\ \delta_3 \\ \delta_4 \end{bmatrix} = \begin{bmatrix} -1 & 1 & 1 & 1 \\ -1 & -1 & 1 & -1 \\ 1 & -1 & 1 & 1 \\ 1 & 1 & 1 & -1 \end{bmatrix} \begin{bmatrix} \delta_{\text{ail}} \\ \delta_{\text{ele}} \\ \delta_{\text{thr}} \\ \delta_{\text{rud}} \end{bmatrix} + \begin{bmatrix} \delta_1^* \\ \delta_2^* \\ \delta_3^* \\ \delta_4^* \end{bmatrix}, \quad (21)$$

where the output $\begin{bmatrix} \delta_1 & \delta_2 & \delta_3 & \delta_4 \end{bmatrix}^T$ are the PWM signals to ESCs and $\begin{bmatrix} \delta_1^* & \delta_2^* & \delta_3^* & \delta_4^* \end{bmatrix}^T$ are the trim values for each motor at the hovering status.

IV. Parameters Identification

Each parameters in the derived model shown in the previous section can be obtained by either software simulation or experimentally.

A. Identification by Experiments

1) Basic Parameters: Parameters that can be directly measured are the mass of aircraft and the length of quadrotor arms. For the gravitational acceleration, in Singapore, which is located at north latitude 2°, is approximated as below:

$$l = 0.058\,\text{m}, \quad (22)$$
$$g \approx 9.781\,\text{m/s}^2. \quad (23)$$

2) Thrust & Torque Coefficient: The thrust and torque coefficient of the rotor can be measured by lever-scale setup, shown in first picture in Fig. 10. An infrared transceiver is fixed beside the rotating propeller to measure the time interval between two adjacent cutting of the propeller. The infrared transceiver is responsive enough that can record as short as 1us. From the time intervals, the real-time angular velocities can be calculated, from which the transient property of the motor is obtained. Thrust can be read from the weighing scale, reflecting the lift force to the mass that has decreased. Thrust vs. square angular speed in RPM is reflected in Fig. 11, and the overall thrust coefficient k_T can be obtained from Eq. 12, which is the slope of the approximate line.

The overall torque coefficient of the rotor can also be measured by a similar setup, shown in the second picture in Fig. 10. The torque is reflected to the weight reduction read from the scale. Figure 12 is obtained similarly to illustrate the relationship between overall torque coefficient k_Q vs. Ω^2.

Finally, the two coefficients are calculated as below:

$$k_T = 3.334 \times 10^{-8}\,\text{N}/(\text{rad}^2/\text{s}^2), \quad (24)$$
$$k_Q = 1.058 \times 10^{-10}\,\text{Nm}/(\text{rad}^2/\text{s}^2). \quad (25)$$

3) Brushed Motor Dynamics: Another experiment is conducted to measure the parameters in brushed motor dynamics. An ArduIMU is used to feed constant input or step input to the brushed ESC to find the minimum value δ_{min} to drive brushed motor as well as the maximum value δ_{max}. Notice that the battery voltage also affects the angular speed and

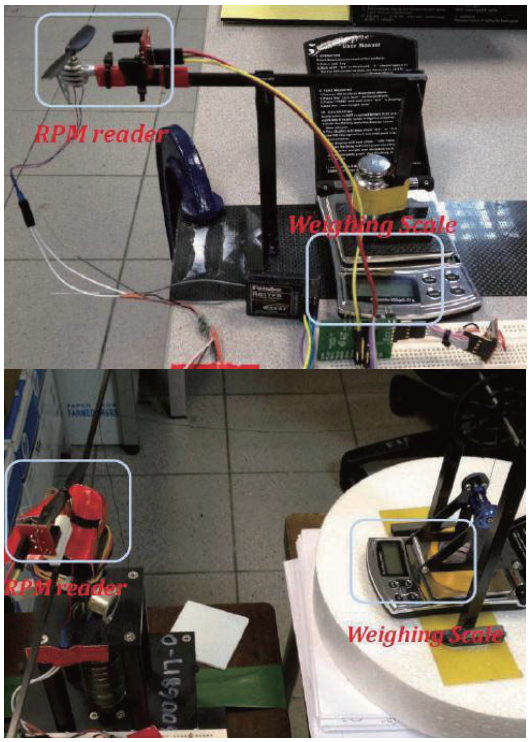

Fig. 10. Experiment setup for measurement of thrust and torque coefficient

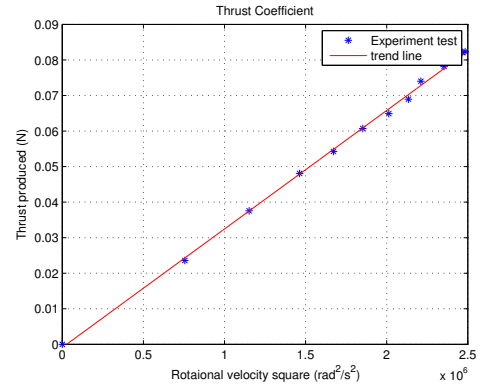

Fig. 11. Thrust against square of motor rotational speed

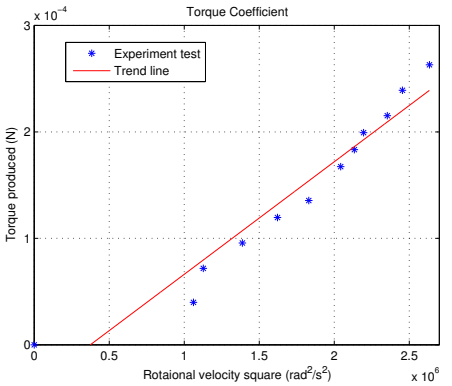

Fig. 12. Torque against square of motor rotational speed

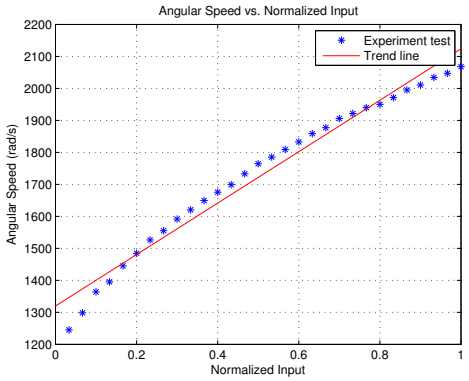

Fig. 13. Motor's angular speed against PWM input

this experiment is done under voltage of 3.8 V. Here it is found that:

$$\delta_{min} = 1050\,\mu\text{s}, \tag{26}$$
$$\delta_{max} = 1800\,\mu\text{s}, \tag{27}$$

and the ESC input is normalized to scale $\Delta_i \in [0,1]$ $(i = 1,2,3,4)$ using the formula below:

$$\Delta_i = \frac{\delta_i - \delta_{min}}{\delta_{max} - \delta_{min}}, \tag{28}$$

where δ_i is the PWM input in unit μs. The rotor starts rotating with PWM value of δ_{min} and saturates at highest speed with value of δ_{max}. The motor's steady state velocity is assumed to be proportional to the input value. Figure 13 shows relationship between the motor's angular speed and normalized PWM input, and the gradient k_m can be extracted from the approximate line:

$$\Omega_{ss} = k_m \Delta_i + \Omega_{min}, \tag{29}$$
$$= 715.9\Delta_i + 1428.5, \tag{30}$$

where Ω_{ss} is the steady state rotational speed, Ω_{min} is the y-intercept of the trend line.

Also, as presented in Eq. 20, the motor dynamics can be approximated as a first-order process:

$$\dot{\Omega}_i = \frac{1}{\tau_m}[k_m \Delta_i - (\Omega_i - \Omega_{min})], \tag{31}$$

where average time constant τ_m is estimated from the approximate model with several step inputs:

$$\tau_m = 0.0821\,\text{s}. \tag{32}$$

B. Identification by Simulations

Some of the parameters are not easily measured with simple experimental set-up, including the inertia tensor of the overall platform and the propeller, and mathematical method is more appropriate to estimate these values.

1) Inertia Moment of Body: With the aid of a 3D simulation program, SolidWorks, real density properties of each component is assigned to the parts in the simulation. The software can then be commanded to calculate its body moment of inertia, as

$$J = \begin{bmatrix} 3.0738 & 0 & 0 \\ 0 & 3.0849 & 0 \\ 0 & 0 & 5.9680 \end{bmatrix} \times 10^{-5}\,\mathrm{kgm}^2, \qquad (33)$$

where the coupling terms are eliminated based on the x-axis and y-axis symmetry.

2) Inertia Moment of Rotor: The basic size information of the propeller is listed in Table. II and Fig. 2(b) shows the simulated rotor in Solidworks. J_r is then estimated as below:

$$J_r = 5.897 \times 10^{-8}\,\mathrm{kgm}^2. \qquad (34)$$

Table. IX summarizes the parameters identified.

TABLE IX
PARAMETERS IDENTIFICATION

Parameters	Description	Values
m	Overall weight	0.0418 kg
g	Gravitational acceleration	9.781 m/s^2
l	CF beam length	0.058 m
k_T	lift coefficient	3.334×10^{-8} N/(rad^2/s^2)
k_Q	Torque coefficient	1.058×10^{-10} Nm/(rad^2/s^2)
δ_{min}	Minimum PWM input	1050 μs
δ_{max}	Maximum PWM input	1800 μs
k_m	Gain of angular speed to normalized throttle	715.9
τ_m	Time constant of the motor dynamic	0.0821 s
J_{XX}	Inertia moment of body about x-axis	3.0738×10^{-5} kgm^2
J_{YY}	Inertia moment of body about y-axis	3.0849×10^{-5} kgm^2
J_{ZZ}	Inertia moment of body about z-axis	5.9680×10^{-5} kgm^2
J_r	Inertia moment of rotor	5.897×10^{-8} kgm^2

V. SIMULATION AND FLIGHT TEST

A. Simulation

Fig. 14 shows the overview of a simple proportional-integral-derivative (PID) control method for the quadrotor's inner loop (attitude control loop) [12]. Since the dynamics of a quadrotor without orientation stabilizer is too fast even for a skilled pilot, the inner loop control is indispensable for orientation stabilization. With the aid of Matlab Simulink, the model discussed in Section III was simulated with PID controller implemented. The PID gains are tuned based on an experimental setup, which is a single-rotating-axis setup

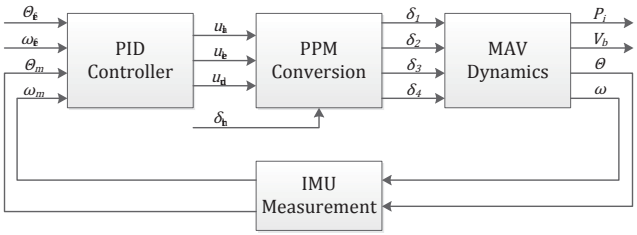

Fig. 14. PID attitude control structure

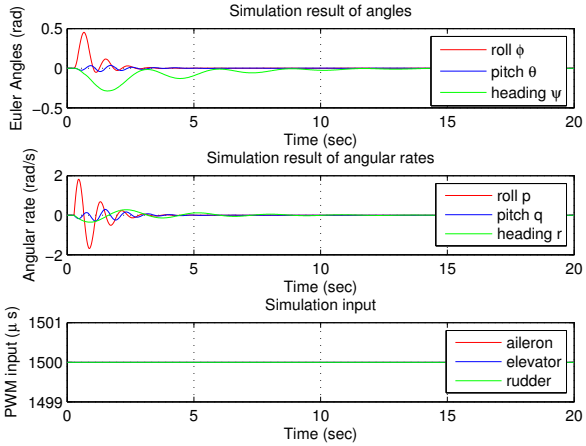

Fig. 15. Simulation results for PID control

to test yaw, pitch and roll separately. As shown in Fig. 16, the quadrotor was able to rotate at only one axis, so that PID gains can be tuned on that single channel.

Gain tuning method is based on Ziegler-Nichols (ZN) method: (i) tuning K_p with K_d and K_i equal to zero such that the Euler angle shows sustained oscillation; (ii) recording the ultimate proportional gain K_u and oscillation period T_u; (iii) adjusting PID gains bsed on ZN rules. $K_u = 2.2$ and $T_u = 1.30$ s for pitch and roll channels are obtained from the plotted graphs of the experiment data. The PID gains are further calculated based on ZN classic PID rule and tuned on the experimental setup shown in Fig. 16. Since it is assumed that the pitch channel and the roll channel are symmetrical with all the parameters identical, the PID gains for roll channel are also the same values.

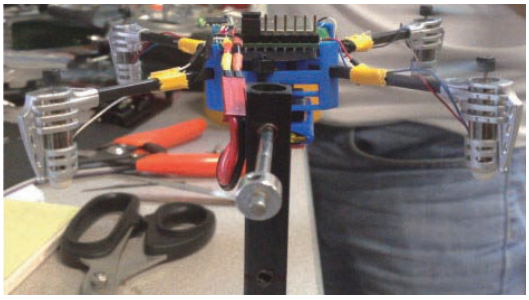

Fig. 16. PID tuning setup for pitch and roll channel

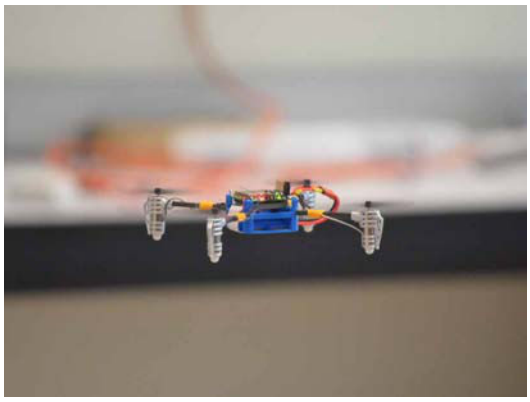

Fig. 17. Full workable prototype quadrotor MAV

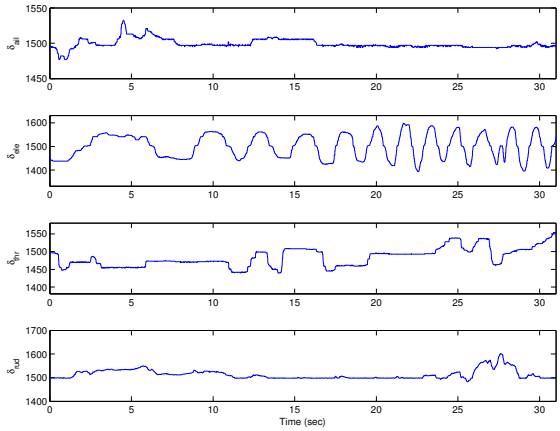

Fig. 18. Input chirp signals for pitch channel

B. Model Verification

The PID controller designed with Simulink was implemented to the well-assembled quadrotor platform and further tuned based on the real flight performance. Flight endurance was tested that a 360 mAh battery was able to last for 8 minutes. Fig. 17 shows the MAV in hovering condition, while orientation stabilization is achievable with satisfactory performance.

In order to verify the nonlinear model derived by the physical working principle, response from chirp signal input was compared with the simulation results. The input chirp signals was recorded by a onboard data logger and the inner loop updating rate is 100 Hz. Fig. 18 and Fig. 20 show the chirp signal in elevator channel and heave channel. The recorded perturbation signals were then fed to the software simulator and simulated output in time domain can be obtained. In the experimental setup, a VICON Motion Capture System is used for measuring the aircraft's global positions and computing the angles as well as the angular rate. In the flight test, the pitch angle and angular rate were logged and plotted to compare with the simulated results in Fig. 19 and Fig. 21.

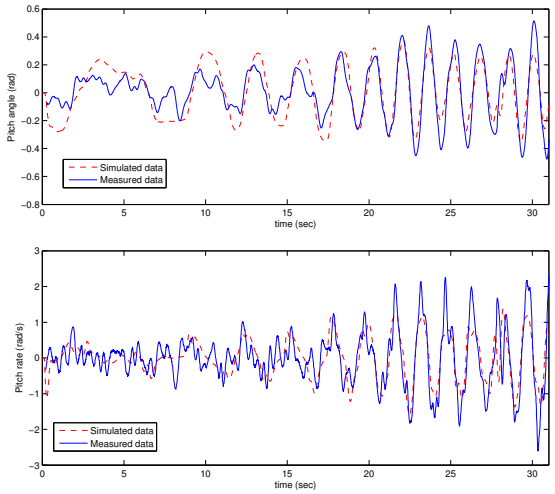

Fig. 19. Model verification of pitch angle and angular rate

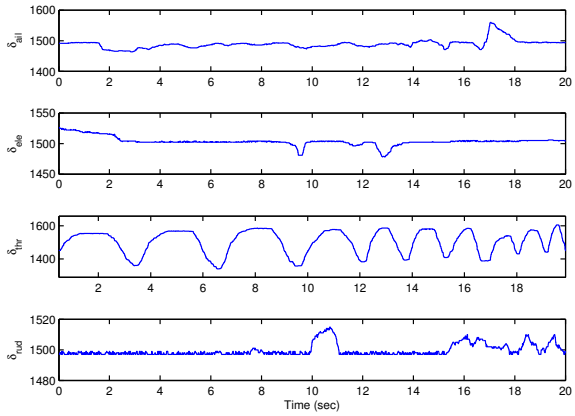

Fig. 20. Input chirp signals for heave channel

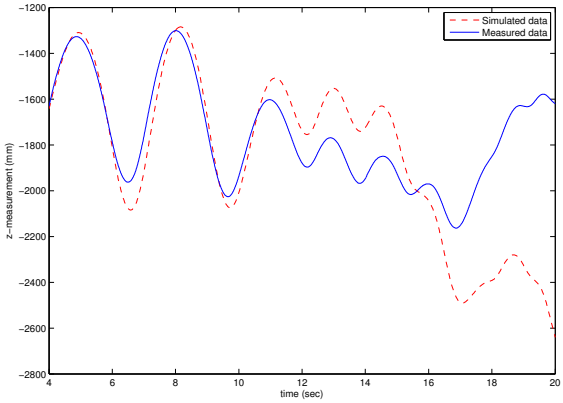

Fig. 21. Model verification of z-axis position

VI. CONCLUSIONS

This paper focuses on a systematic design method of an ultralight quadrotor MAV. Based on the project requirements, mechanical system design, structural analysis, electrical system design along with components selection are conducted and scrutinized in sections. Then a mathematic model is constructed with respect to flight kinematics, 6 DOF rigid body dynamics, forces and moments generation as well as motor dynamics. To identify the parameters in the mathematical model, some experiments are set up to measure and analyze these values. Moreover, a simple yet reliable PID controller is simulated with software simulator first and implemented to the platform. The flight test results shows the orientational stability as well as the reliability of the nonlinear model. Further development would be carried out on robust controller on both inner loop and outer loop of the quadrotor MAV that would reject the disturbance from environment and track desired trajectories.

REFERENCES

[1] J.M. Grasmeyer, and M.T. Keennon, "Development of the black widow micro air vehicle", *Progress in Astronautics and Aeronautics 195*, pp. 519-535, 2011.

[2] R.J. Wood, "Design, Fabrication and Analysis of a 3DOF, 3cm flapping-wing MAV", *Proceedings of the 2007 IEEE/RSJ International Conference on Intelligent Robots and Systems San Diego*, CA, USA, Oct 29-Nov 2, 2007.

[3] R. Naldi, L. Gentili, L. Marconi and A. Sala, "Design and Experimental Validation of a Nonlinear Control Law for a Ducted-Fan Miniature Aerial Vehicle", *IEEE Transactions on Control Systems Technology*, 2008.

[4] I. Kroo and P. Kunz, "Mesoscale Flight and Miniature Rotorcraft Development", *American Institute of Aeronautics and Astronautics*, Jan, 2010.

[5] D. Mellinger, M. Nathan and V. Kumar, "Trajectory generation and control for precise aggressive maneuvers with quadrotors", *The International Journal of Robotics Research*, vol. 31(5), pp. 664-674, 2012.

[6] F. Wang, S. K. Phang, J. Cui, B. M. Chen and T. H. Lee, "Nonlinear Modeling of a Miniature Fixed-Pitch Coaxial UAV", *American Control Conference*, Fairmont Queen Elizabeth, Montreal, Canada, June 27-29, 2012.

[7] S. Bouabdallah, A. Noth and R. Siegwart, "PID vs LQ Control Techniques Applied to an Indoor Micro Quadrotor", *IEEE International Conference on Intelligent Robots and Systems*, pp. 2451-2456, 2004.

[8] R. Mahony, V. Kumar, P. Corke, "Multirotor Aerial Vehicles: Modeling, Estimation, and Control of Quadrotor", *IEEE Robotics & Automation Magzine*, pp. 20-32, Sep 2012.

[9] G. Cai, B. M. Chen and T. H. Lee, *Unmanned Rotorcraft Systems*, Springer, 2011.

[10] R. Goel, S. M. Shah, N. K. Gupta and N. Ananthkrishnan, "Modeling, Simulation and Flight Testing of an Autonomous Quadrotor", *Proceedings of International Conference on Environmental and Agriculture Engineering*, 2009.

[11] P.Pounds, R.Mahony, J.Gresham, P.Corke and J.Roberts, "Towards dynamically-favourable quadrotor aerial robots", *Proceedings of the Australian Conference on Robotics and Automation*, Canberra, Australia, 2004.

[12] S. K. Phang, C. Cai, B. M. Chen and T. H. Lee, "Design and mathematical modeling of a 4-standard-propeller (4SP) quadrotor", *Proceedings of the 10th World Congress on Intelligent Control and Automation*, Beijing, China, pp. 3270-3275, July 2012.